nuclear fusion
IAEA

PAPER • OPEN ACCESS

Observation and interpretation of tornado modes coupled to near-axis Alfvén cascade eigenmodes in JET sawtoothing plasmas

To cite this article: R. Calado *et al* 2022 *Nucl. Fusion* **62** 066019

View the article online for updates and enhancements.

You may also like

- Advances in applications of the physics of fluids to severe weather systems
Howard B Bluestein
- Daily tornado frequency distributions in the United States
J B Elsner, T H Jagger, H M Widen et al.
- ARE GIANT TORNADOES THE LEGS OF SOLAR PROMINENCES?
Sven Wedemeyer, Eamon Scullion, Luc Rouppe van der Voort et al.

This content was downloaded from IP address 1.27.104.22 on 03/11/2023 at 09:30

OPEN ACCESS
IOP Publishing | International Atomic Energy Agency Nuclear Fusion
Nucl. Fusion **62** (2022) 066019 (8pp) https://doi.org/10.1088/1741-4326/ac514d

Observation and interpretation of tornado modes coupled to near-axis Alfvén cascade eigenmodes in JET sawtoothing plasmas

R. Calado[1,*], F. Nabais[1], S.E. Sharapov[2], João P.S. Bizarro[1,a] and JET Contributors[b]

[1] Instituto de Plasmas e Fusão Nuclear, Instituto Superior Técnico, Universidade de Lisboa, 1049-001 Lisboa, Portugal
[2] CCFE, Culham Science Centre, Abingdon OX14 3DB, United Kingdom of Great Britain and Northern Ireland

E-mail: rui.p.calado@tecnico.ulisboa.pt

Received 15 October 2021, revised 11 January 2022
Accepted for publication 2 February 2022
Published 5 April 2022

Abstract

The coupling between upwards frequency sweeping modes and tornado modes observed in a set of JET sawtoothing discharges is investigated. The frequency sweeping modes are identified as near-axis Alfvén cascade (AC) eigenmodes. These ACs are associated with a very flat but monotonic q-profile near the magnetic axis, in contrast to the usual reversed-shear scenarios. The frequency evolution of the modes during gradual decrease of the q-profile is numerically reproduced and the transition from cascade modes to tornado modes is demonstrated. The transition occurs for specific values of q on-axis given by $q_0 = (n - 1/2)/n$ and is marked by the characteristic tip of the tornado modes' frequency evolution pattern observed in spectrograms. Based on this result a novel MHD spectroscopy technique is proposed to track the evolution of q_0 in the post sawtooth crash regime with high accuracy by using tornado mode tips as MHD markers, the only requirement being that the toroidal mode numbers are measured. Additionally, calculation of the resonant interaction between the modes and an ICRH-heated hydrogen minority population shows the ions transferring their energy to the modes, thus contributing to the mode drive.

Keywords: tokamaks, Alfvén eigenmodes, MHD spectroscopy

(Some figures may appear in colour only in the online journal)

1. Introduction

Strong wave–particle interaction in magnetic fusion has been shown to be responsible for exciting Alfvén instabilities and worsening the confinement of energetic ions in tokamak plasmas [1, 2]. Energetic ions have their origin either in fusion reactions, as is the case with alpha particles, or via auxiliary plasma heating schemes, such as neutral beam injection (NBI) and ion cyclotron resonance heating (ICRH) [3]. The plasma core region is of particular interest, not only because it is where most fusion reactions will take place but also due to both NBI and ICRH heating schemes being most often tuned for on- or near-axis heating.

Alfvén instabilities are usually observed as a discrete spectrum of Alfvén eigenmodes (AEs). Aside from the original interest regarding the impact of such instabilities on energetic ion confinement, the observed AE spectra can be used for MHD spectroscopy [4–6]. In particular, the observation of Alfvén cascades (ACs) provides information on the evolution of the minimum of the safety factor profile $q_{\min}(t)$ [5, 7] in advanced tokamak scenarios. Although probing the near-axis region of tokamak plasmas is challenging for most

* Author to whom any correspondence should be addressed.
[a] Died January 04, 2022.
[b] See Joffrin *et al* 2019 (https://doi.org/10.1088/1741-4326/ab2276) for the JET Contributors.

© 2022 The Author(s). Published on behalf of IAEA by IOP Publishing Ltd
Printed in the UK

This is an open access article distributed under the terms of the Creative Commons Attribution 4.0 License.
Any further distribution of this work must maintain attribution to the author(s) and the title of the work, journal citation and DOI.

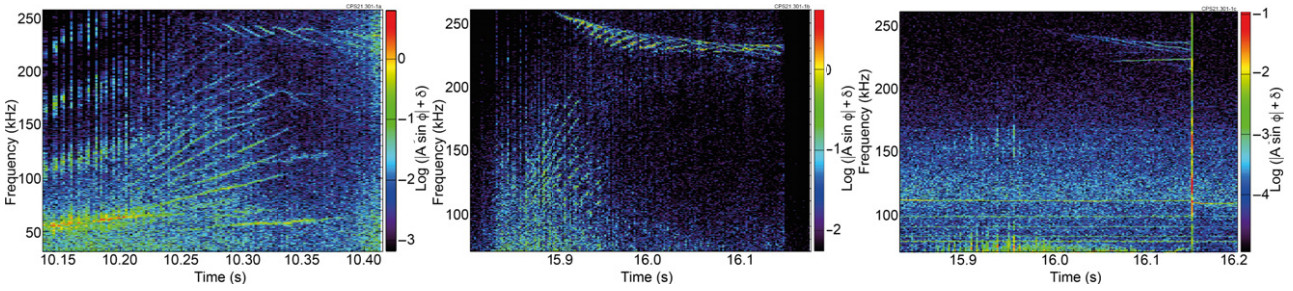


Figure 1. Spectrograms of density perturbations from O-mode interferometry on JET discharges No. 66206 (*a*) and 66203 (*b*). Tornado modes are visible in the frequency range around 225–250 kHz while AC type modes are seen sweeping in the frequency range 100–200 kHz in (*a*) and 100–225 kHz in (*b*). (*c*) Magnetic spectrogram of the same discharge and approximate time interval as in (*b*). Only a fraction of the tornado modes observed in (*b*) is detected with magnetic diagnostics, while ACs are not detected.

diagnostics, internal diagnostics such as interferometry techniques [8, 9] are able to detect Alfvénic activity close to the magnetic axis. Observation of AEs may in turn be employed for MHD spectroscopy of core plasma parameters such as the safety factor profile. MHD spectroscopy plays an important role as a 'diagnostic' providing both qualitative and quantitative details of plasma evolution. Two main types of AEs are described in this study. Tornado modes are one of the AE types. These core-localised modes were first reported from TFTR experiments with ICRH applied to sawtoothing plasmas [9, 10]. Similar studies performed then on JT-60U [11] have concluded that such modes are more harmful for energetic ion confinement than usual global TAEs. Because the frequencies of such modes with different toroidal mode numbers were forming a specific pattern with time, these modes were nick-named 'tornado modes' [11]. Theoretical investigation [12] has shown that the part of tornado frequency sweeping down can be explained by a minor temporal evolution of the on-axis safety factor $q_0(t)$. An alternative interpretation of the tornado frequency sweeping was proposed in [13] where the concept of energetic particle modes was considered. Finally, the observation of two sets of tornado modes excited simultaneously at frequencies close to the top of TAE-gap and the bottom of TAE-gap in a JET experiment allowed performing an unambiguous identification of the tornado modes [14]. It was demonstrated that the modes are TAEs inside the $q = 1$ radius, mode structures and frequencies of which are affected by the proximity of the magnetic axis, thus explaining the unusual temporal evolution of the mode frequency at minor changes in $q_0(t)$ (as was originally proposed in [12]). The effect of tornado modes on re-distribution of energetic ions at the plasma center was experimentally established in [15, 16]. The other AE type consists of ACs. These modes are associated with shear reversed [5, 7, 17] or, in some conditions, sufficiently flat [18–20] q profiles.

In the present paper, we investigate O-mode interferometry observations from a set of sawtoothing discharges on the JET tokamak exhibiting the coexistence of tornado modes and ACs. These modes, especially the latter, are weakly or even not at all detected in standard magnetic diagnostics, suggesting they are localized very close to the magnetic axis. While tornado modes have been identified and investigated in detail in [21], the AC modes have not been studied. Interestingly, spectrograms suggest a connection between these two types of modes. It is the aim of this paper to report on the observation of these near-axis AEs and to provide an explanation and modelling of the two families of modes and their coupling. Furthermore, we investigate the possibility of developing an MHD spectroscopy technique based on these modes that provides information on the safety factor evolution in sawtoothing plasmas.

The paper is organised as follows. In section 2 we present the experimental observations. Section 3 contains the results from the modelling work. The numerical calculation of the modes frequency and radial structure is presented and an MHD spectroscopy technique for the post-sawtooth crash evolution of the q profile is proposed based on the results. Additionally, we present calculations of the mode drive due to the presence of a minority population heated by ICRH. In section 4 we summarize the results and draw conclusions from the work.

2. Experimental observations

Figures 1(*a*) and (*b*) show spectrograms of electron density perturbations detected via O-mode interferometry from two discharges on the same experimental session, which was dedicated to the study of tornado modes. Tornado modes are visible in the frequency range 225–250 kHz and comprise a sequence of modes with toroidal mode number n decreasing in time one-by-one, i.e. higher n tornado modes being observed first [12]. ACs experience an upwards frequency sweep starting from around 80–100 kHz. The existence of multiple branches suggests the presence of a so-called grand cascade originated at an integer $q_{\min}$ value. Results from previous work [14] localizing the tornado modes inside the $q = 1$ surface further suggest that the grand cascade is associated with $q_{\min} = 1$ [7]. During sawtooth crashes, magnetic reconnection causes q on axis, q_0, to jump up to values that can be either above or slightly below unity. In this set of discharges, sawtooth crashes that are followed by grand cascades, as the ones observed in figures 1(*a*) and (*b*), result in $q_0 > 1$ and it takes some time for plasma current to diffuse towards the centre and lower the safety factor down to $q_0 < 1$ thenceforth allowing for the grand cascade to exist.

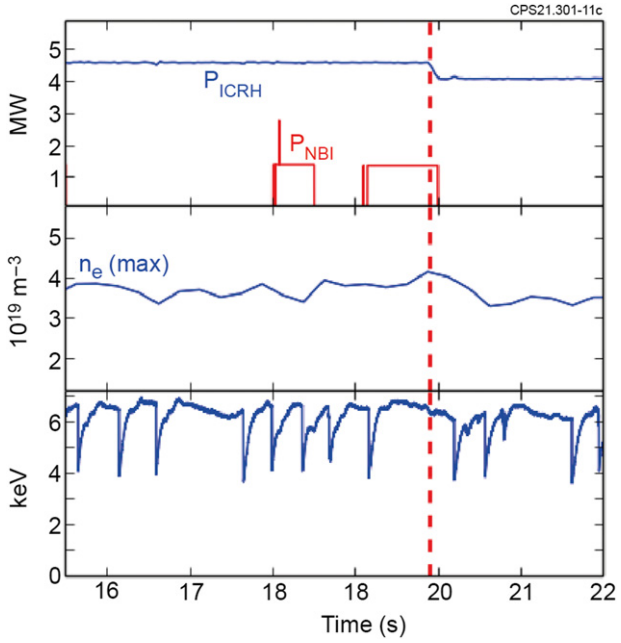


Figure 2. (Top) Power waveforms of ICRH and NBI. (Middle) Maximum electron density measured with LIDAR. (Bottom) Central electron temperature measured with ECE diagnostics. The vertical dashed line marks the time slice considered for the modelling of section 3.

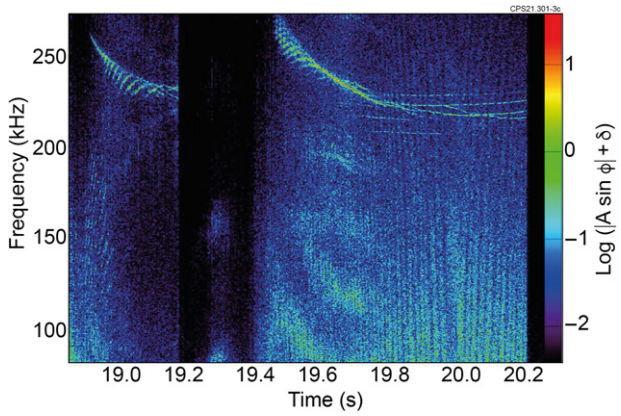


Figure 3. Spectogram of density perturbations measured with O-mode interferometry. Two groups of tornado modes are observed with frequencies in the range 225–250 kHz. The first group is preceded by AC type modes sweeping upwards in frequency in the range 100–200 kHz.

The spectrograms show evidence of the coupling between ACs and tornados, in the sense that AC modes seem to transition into tornado mondes. While figure 1(*b*) exhibits a frequency gap between the two families of modes, the evidence for coupling between the modes is clearer in figure 1(*a*) since some AC modes are observed to sweep upwards until they reach tornado frequencies. Figure 1(*c*) shows the magnetic spectrogram equivalent to figure 1(*b*). The AC and many tornado modes are not detected by the more peripheral magnetic diagnostics. This suggests these modes are located close to the magnetic axis, where only internal diagnostics such as O-mode interferometry are able to probe. The aim of this study is to explain and reproduce numerically the set of modes observed in figure 1(*b*), covering the time interval [15.8; 16.2] s.

Electron temperature measured by a core ECE channel, maximum electron density measured by LIDAR, as well as the power waveforms of ICRH and NBI for JET discharge No. 66203 can be seen in figure 2 for a time interval of interest. This discharge was characterized by a 2 MA plasma current and a 2.7 T magnetic field. Auxiliary plasma heating came from 4 MW ICRH with frequency tuned for on-axis heating of an hydrogen minority population ($n_{\mathrm{H}}/n_{\mathrm{e}} \approx 2.5\%$) while NBI blips were applied for diagnostic purposes, namely motional Stark effect (MSE) measurements. Although these MSE measurements could provide a better insight into the equilibrium profiles in the central region of the plasma allowing for an accurate equilibrium reconstruction of the plasma core region (see, e.g. [22], and references therein), they were employed only at a later time than our observations of interest. We used in our analysis of the modes q-profiles similar to those measured later with MSE but adjusted to the value of total current (value of q_0).

Figure 3 illustrates a spectrogram during a time interval encompassing the NBI blip applied at around $t = 19$ s seen in figure 2. There are two groups of tornado modes observed, but only the first is preceded by AC type modes, while MSE measurements are available for the duration of the second group of tornado modes. The most likely reason for the absence of the grand cascade in the interval [19.3, 19.9] s is that q_0 did not jump above unity during the preceding sawtooth crash. The instant $t = 19.9$ s marked in figure 2 with a red dashed line was selected for the reconstruction of the q-profile.

3. Modelling

3.1. Mode identification and characterization

Modelling of the experimentally observed tornado and AC type modes was performed with the MHD codes HELENA [23], CSMISHKA and MISHKA [24]. The primary goal was to shed light on the apparent coupling between ACs and tornado modes. It was essential that the radial location of both families of modes was identified and the temporal evolution of their frequencies reproduced. We proceeded as follows. Firstly, the equilibrium was reconstructed with EFIT taking into consideration constraints from MSE measurements. Then, HELENA refined the equilibrium. The resulting equilibrium was then provided to CSMISHKA to compute the corresponding Alfvén continuum structure. Finally, the Alfvén continuum gap of interest was scanned for the existence of modes with MISHKA, which computes the mode's frequency and radial structure.

Sawtooth oscillation dynamics dictates that the q profile is expected to decrease during the sawtooth period down to values below unity on axis, followed by a sudden jump during the sawtooth crash. In order to mimic this behaviour, the q profile originated from the reconstructed HELENA equilibrium is rescaled to different on-axis values q_0 for each

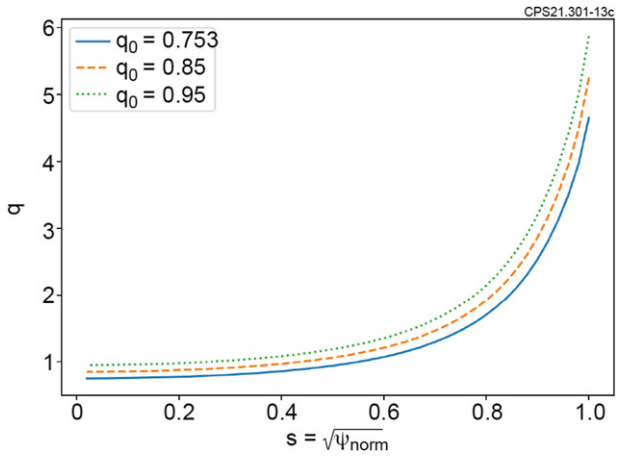


Figure 4. Radial q profile from HELENA rescaled for different values on axis. Solid line: q profile from HELENA equilibrium (no rescaling). Dashed line: q profile rescaled for on-axis value $q_0 = 0.85$. Dotted line: q profile rescaled for on-axis value $q_0 = 0.95$.

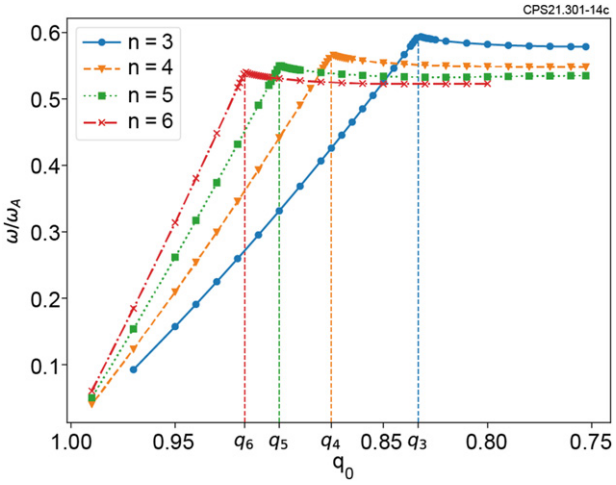


Figure 5. Evolution of the frequency of the modelled modes with q_0 (normalized to the Alfvén frequency $\omega_A \equiv v_A/R_0$). Four toroidal mode numbers are shown: $n = 3$ (blue circles and solid line), $n = 4$ (orange triangles and dashed line), $n = 5$ (green squares and dotted line) and $n = 6$ (red Xs and dash-dotted line). They all exhibit an AC phase and a tornado phase, with the transition occurring when q_0 crosses the q value associated with the TAE gap, q_n.

CSMISHKA and MISHKA run. Decreasing/increasing q_0 represents moving forwards/backwards in time. This method is employed to track the temporal evolution of the mode frequency, structure and location. Figure 4 shows three examples of q profiles rescaled for different q_0. The profile is monotonic but very flat near the axis. Although AC modes are usually associated with magnetic shear reversal, a sufficiently low shear may create a 'potential well' that allows the existence of AC eigenmodes near the plasma centre [17, 18].

The radial structure and frequency of modes with toroidal mode number $n = 3$–6 were computed with MISHKA. Even though the modes were faintly observed by the magnetics, some stretches of the modes do allow measurement of the toroidal mode numbers. In particular, it was possible to identify $n = 5$ and $n = 3$ tornado modes. We build up then the toroidal mode numbers for other modes using the well-established pattern of tornado sequence [12]. These are typical mode numbers for TAEs observed in JET. Figure 5 shows the evolution of the modes' frequencies with q_0. The horizontal axis is intentionally reversed to reproduce the temporal evolution of the safety factor. For all toroidal mode numbers the same two-phase evolution is observed. The first phase strongly resembles a $q_0 = 1$ grand cascade. All mode numbers asymptotically share the same frequency as q_0 approaches unity. As time passes, q_0 decreases and the modes' frequencies rise. Higher mode numbers experience a faster frequency rise. This relationship between mode number and steepness of the frequency rise is well-known for AC modes. In all cases, the frequency rises until it reaches a tipping point from where it starts decreasing slowly. This second phase matches the temporal evolution observed for tornado modes. The transition point occurs when q_0 matches the safety factor value associated with the TAE gap of the tornado given by $q = (m - 1/2)/n$, where m is the poloidal mode number. Since q_0 is taken to be slightly below unity, $m = n$ and the transition safety factor value on-axis is given by $q_0 = q_n = (n - 1/2)/n$. These results suggest the following evolution of the modes along the period between consecutive sawtooth crashes. The first sawtooth crash elevates the safety factor profile in the near-axis region to values above unity. While sawtooth crashes do not necessarily result in $q_0 > 1$, that is the case here since a grand cascade is observed from the start, implying the existence of an integer q surface. As q decreases and crosses $q_0 = 1$ the grand cascade is originated with multiple toroidal mode number AC branches being observed. The frequency of each AC mode increases until q_0 crosses the transition q_n value. At that time, the AC is converted into a tornado mode and its frequency slowly decreases as q continues to decrease. The evolution is stopped by the second sawtooth crash that brings q_0 back up again to values above unity and the cycle is repeated.

Figure 6 shows the evolution of the mode's structure and radial position of the $n = 4$ mode. Figures 6(a) and (b) show the mode's structure during the AC phase, which can be recognized by the single dominant poloidal harmonic [18] $m = n = 4$. Figures 6(c) and (d) show the mode's structure in two time slices of the tornado phase. In this phase, the mode is dominated by the pair of poloidal harmonics $m = n = 4$ and $m = n - 1 = 3$. We can establish the evolution of the mode's structure as follows. A narrow AC mode is excited as part of a grand cascade very close to the magnetic axis shortly after the safety factor on axis crosses unity. As the plasma core safety factor decreases, the near-axis AC mode moves radially outwards and broadens. When q_0 crosses $q_4 = 0.875$ there is a transition to a tornado phase during which the mode continues moving outwards as q_0 decreases, following the migration of the TAE gap formed at the transition. The tornado modes have a much larger radial extent than the AC modes. Similar evolution is observed for $n = 3, 5, 6$ modes. The distance of the modes to the plasma edge during the AC and early

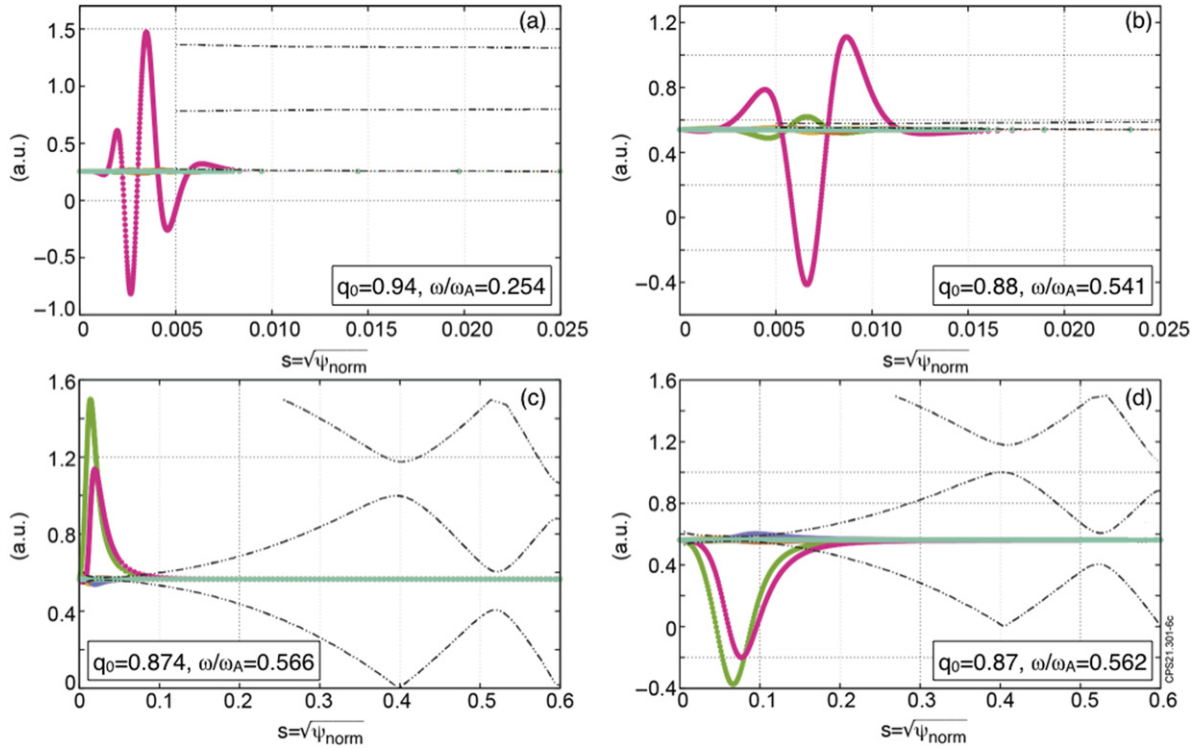


Figure 6. Evolution of the $n = 4$ mode's structure, radial position and frequency with q_0. Temporal evolution is represented from left to right, top to bottom, that is, decreasing q_0 value. Top figures show cascade mode with a single dominant poloidal harmonic $m = n = 4$. Bottom figures show tornado mode with a pair of dominant harmonics $m = 3, 4$ (green and magenta, respectively). We point out the different scaling and range in the horizontal axis between top and bottom figures, necessary due to the different scale width of the mode during AC and tornado phases. Mode starts from very close to the axis and gradually moves outwards. Dash-double-dotted lines represent the Alfvén continuum. Ψ_{norm} is the magnetic flux normalized to the value on the last closed flux surface.

tornado phases is consistent with the observation that magnetic diagnostics are only able to detect late-stage tornado modes.

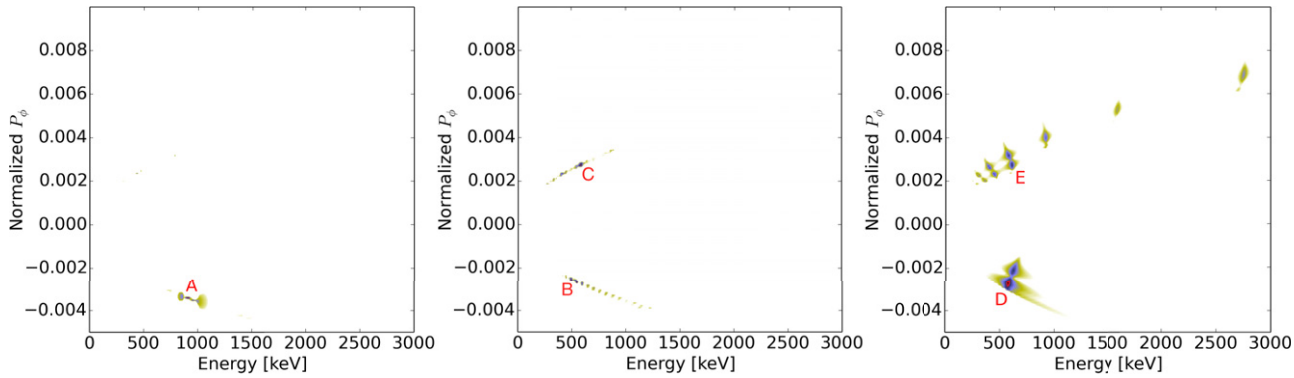
3.2. MHD spectroscopy of q_0

After the sawtooth crash, q_0 is known to gradually decrease. Figure 5 shows the slope of the evolution of mode's frequency transitioning from upward sweeping to downward sweeping exactly when q_0 crosses the critical value q_n. These transition points may therefore serve as important markers for estimation of post-sawtooth evolution of q_0. We note that they are usually observed in tornado modes even in the absence of the near-axis grand-cascades. In particular, such points were found in the frequency evolution of tornado modes presented in [14], but no specific interpretation was provided for these. The observation of near-axis grand-cascades provides additional information on q_0 immediately after sawtooth crashes since they require the safety factor to be elevated above unity, whereas when they are not observed no conclusion may be drawn because it may be due to other factors such as insufficient drive.

3.3. Particle drive

The CASTOR-K code [25] is a linear drift-kinetic code that was used to identify the resonant ions driving each type of mode and assess the overall damping or drive effect of the energetic ions population on tornado and AC modes. Ion orbits are identified by a set of three constants of motion: energy, E, toroidal canonical momentum $P_\phi = Ze\Psi + m_i v_\parallel RB_\phi/B$, Ze and m_i representing the energetic ion charge and mass, respectively, and Ψ the poloidal magnetic flux, and normalized magnetic moment $\Lambda = \mu B_0/E$, where μ is the magnetic moment and B_0 the magnetic field on axis. In this discharge, ICRH frequency was tuned for resonance at $B_{\text{res}}/B_0 = 0.96$ and a population characterized by a single normalized magnetic moment $\Lambda = 0.96$ was considered. These energetic ions are distributed in the (E, P_ϕ) phase-space following a distribution that was assumed to be Maxwellian, with temperature peaked on axis and peak value of 527 keV [21]. The radial density profile was peaked in the centre and in the simulations a function given by $\rho = \rho_0(1 - s^2)^2$ was used, where s is the square root of the poloidal flux normalized to the flux on the last closed flux surface. Each (E, P_ϕ) pair, together with $\Lambda = 0.96$, defines an orbit for which CASTOR-K computes the energy exchange between the ion and the mode.

Figure 7 shows the energy exchange as a function of (E, P_ϕ) for three time slices corresponding to different phases of the $n = 4$ mode (namely, low-frequency AC, high-frequency AC just before the transition and tornado mode after the transition). The colour scale was chosen to allow a clear identification of the orbits driving each mode. P_ϕ is shown normalized to $P_{\phi 0} = ZeB_0R_0^2$. Damping interactions are suppressed in the figures so that resonant ions driving the mode can be more clearly identi-



(a) $q_0 = 0.94$ (b) $q_0 = 0.88$ (c) $q_0 = 0.87$

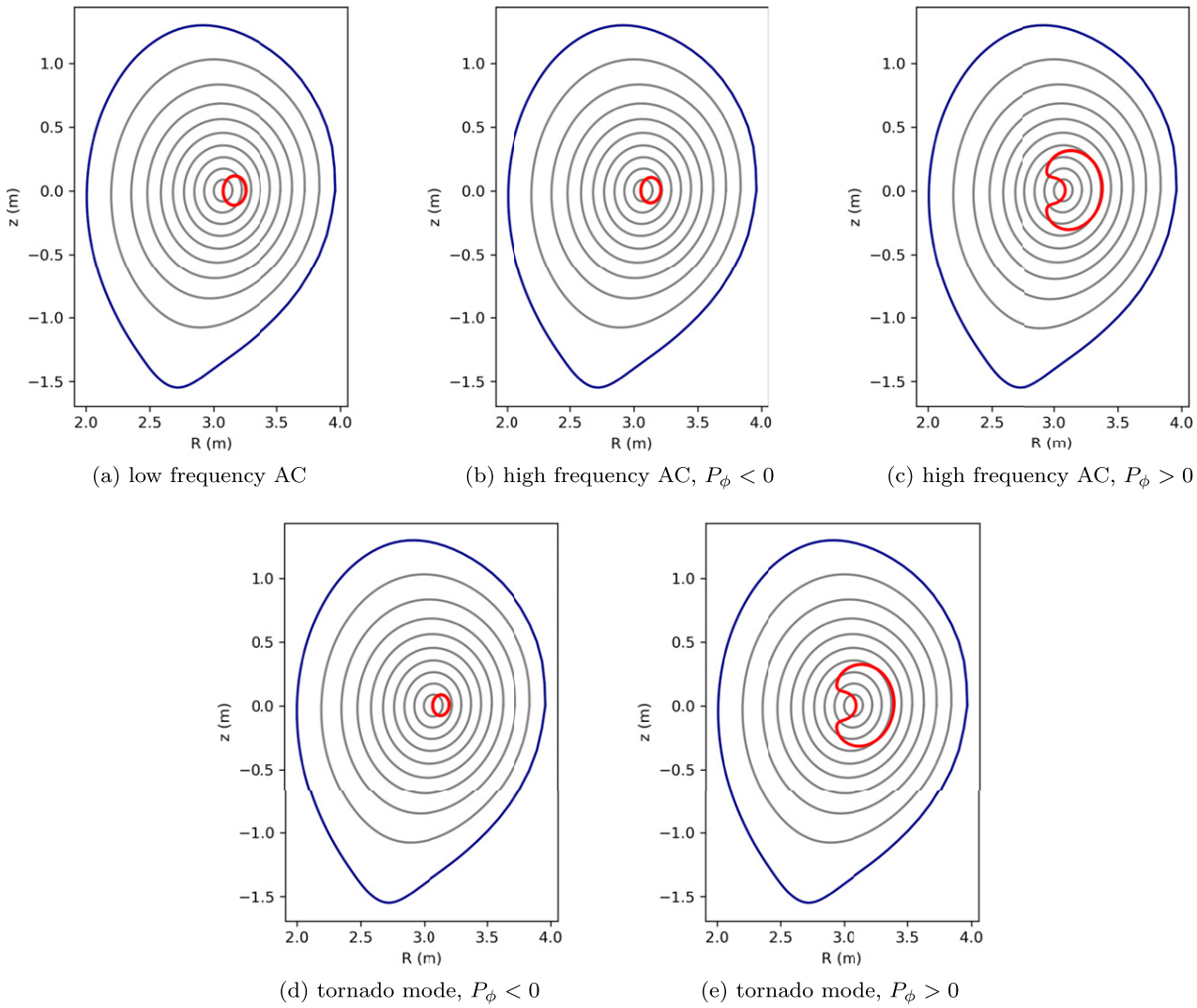
Figure 7. Energy exchange contributing to drive of the $n = 4$ mode as a function of (E, P_ϕ) in three stages of mode evolution. Figures (a)–(c) correspond to the modes displayed in figures 6(a), (b) and (d), respectively. The tornado mode resonantly interacts with the ions over a wider range of energy and resonances are broader in P_ϕ (resonances D and E) than in the case of cascades (resonance A in the low frequency AC and resonances B and C in the high frequency AC). The orbits of ions in the resonances identified by A–E are shown in figure 8.

fied. Figures 7(a)–(c) display the resonances computed for the modes exhibited in figures 6(a), (b) and (d), respectively. During the tornado phase the mode is being driven by several resonance lines. The only resonance driving the mode with $P_\phi < 0$ is in the energy range 500–700 keV and is the dominant interaction. Additional significant resonances exist for $P_\phi > 0$ and extend over a wider range of energies, starting from around 250 keV and extending up to approximately 2.75 MeV. A stark difference between the tornado and the AC cases is the highly localized nature of the energy exchange in P_ϕ observed in the latter. To understand this result one must acknowledge that the toroidal canonical momentum can be viewed as a radial coordinate. This is particularly clear when one considers the tip of standard banana orbits for ions accelerated by on-axis ICRH heating where $v_\parallel = 0$, meaning that $P_\phi = Ze\Psi$ is proportional to the common radial coordinate Ψ of the tip. Therefore, given the very narrow radial structures of the AC modes shown in figures 6(a) and (b) they are only able to interact with ions in very restricted P_ϕ ranges. The high-frequency AC exhibits strong energy exchange with ions of energies around 500 keV and $P_\phi < 0$ as well as energies approximately in the range 400–600 keV and $P_\phi > 0$. Different resonance lines are not clearly distinguished. However, the high-frequency AC and the tornado mode have similar frequencies and as such they are expected to share approximate resonance lines. By comparison of figures 7(b) and (c) we can infer that the region of interaction for $P_\phi > 0$ crosses multiple resonance lines. As for the case of the low frequency, only a single resonance shows significant wave-particle energy exchange. These ions move in potato orbits with energies around 900 keV.

The orbits corresponding to the most significant resonances shown in figure 7 are drawn in figure 8. The results presented in section 3 show us the modes are very localized near the axis. Furthermore, the ICRH accelerated population is very peaked at the magnetic axis. Thus, the orbits relevant to wave–particle interactions between the AEs and the ICRH population are close to the axis. Figures 8(a), (b) and (d) show the orbits corresponding to the resonances with $P_\phi < 0$ of the low frequency cascade, the high frequency cascade and the tornado mode, respectively. They are non-standard orbits, varying from one mode to the other mainly in width in accordance with the different energies at which the resonance occurs for each mode. Figures 8(c) and (e) show the orbits of the $E \approx 600$ keV, $P_\phi > 0$ resonances of the high frequency cascade and the tornado mode. The orbits are very similar in the cases of the high-frequency AC and the tornado mode as they approximately share the same resonances, differing mainly in radial extent.

The overall mode damping or drive results from integration of the individual ion orbits' results over the relevant occupied phase space shown in figure 7. In all three stages being considered the energetic population was found to drive the mode. The computed growth rates normalized to mode frequency, γ/ω, using the assumed energetic ion distribution, were 0.196% and 0.0168% for the low- and high-frequency ACs, respectively, and 3.07% for the tornado mode. The tornado mode experiences stronger drive since it is able to interact over a wider range of the (E, P_ϕ) phase space due to its larger radial extent. It is interesting, however, to note that the drive experienced by the high-frequency AC is an order of magnitude lower than that of the low-frequency AC. The lower drive from the energetic ion population may explain the frequency gap observed between AC and tornado modes in figures 1(b) and 3, as competing damping mechanisms possibly overcome ion drive resulting in overall damping of the mode during this stage.

We note here that the effect of finite Larmor radius of the energetic ions should affect the estimate of the drive of the modes strongly localized radially [26], namely the AC modes. Nevertheless, such effect, although reducing the energy exchanged from the energetic ions to the mode, cannot change the positive sign of the drive.



(a) low frequency AC (b) high frequency AC, $P_\phi < 0$ (c) high frequency AC, $P_\phi > 0$

(d) tornado mode, $P_\phi < 0$ (e) tornado mode, $P_\phi > 0$

Figure 8. Orbits of the ions most strongly driving the modes as identified in figure 7. Figure (*a*) corresponds to resonance A from figure 7(*a*); figures (*b*) and (*c*) correspond to resonances B and C from figure 7(*b*), respectively; figures (*d*) and (*e*) correspond to resonances D and E from figure 7(*c*). The orbits are non-standard and close to the magnetic axis. The high-frequency AC and the tornado mode interact with ions following similar orbits, as expected from the similar frequencies and radial position of the modes.

4. Conclusions

The spectrograms of electron density perturbations detected via O-mode interferometry in a set of JET discharges exhibit a seeming coupling between upwards frequency sweeping modes resembling ACs and modes in the TAE frequency range identified in [21] as tornado modes. In the present work, a set of MHD codes was used to determine the radial location of both types of modes and numerically reproduce their frequency evolution. The frequency sweeping modes were identified as near-axis ACs associated with a very flat yet monotonic q-profile close to the magnetic axis. Although the existence of cascade modes in a flat monotonic q-profile has been theoretically demonstrated in the past [18, 19], this work represents the first numerical identification of such modes in JET discharges. The frequency evolution of the modes was reproduced by successively rescaling the q-profile to mimic the gradual decrease after a sawtooth crash. It was observed that as q decreases, the cascade modes sweep upwards in frequency until the TAE range is reached where they transition to tornado modes. The transition was found to take place when q_0 crosses the $m = n$ TAE characteristic value $q_n = (n - 1/2)/n$. This result is proposed to be used as a novel MHD spectroscopy technique to track q-profile evolution after a sawtooth crash where observation in spectrograms of AC to tornado transitions can be used as markers of q_0 taking known values. The only requirement is that the characteristic tips of tornado modes, which mark the transition from an AC to a tornado mode, are observed in spectrograms originated from magnetic diagnostics, in which case we know both the instant of the transition and the toroidal mode number of the mode.

Regarding the radial structure of the modes, it was observed that AC modes are highly localized, in contrast with the larger radial extent of the tornado modes. Nevertheless, both modes were found to reside close to the magnetic axis, with cascades closer to the axis than tornado modes.

The present work also contemplated the energy exchange between the modes and an energetic hydrogen minority population accelerated by ICRH. The results show the ion population contributes to mode drive. AC modes were observed to interact over resonances with very narrow P_ϕ ranges, while tornado modes exchange energy in broader resonances, as expected due to their larger radial extent. The significant resonances observed identify ions following non-standard orbits close to the magnetic axis. The drive was found to be stronger for tornado modes and lower for ACs just before the transition. The weaker drive experienced by the latter is a probable explanation for the experimentally observed gap between ACs and tornado modes.

Acknowledgments

This work has been carried out within the framework of the EUROfusion Consortium and has received funding from the Euratom research and training programme 2014–2018 and 2019–2020 under Grant Agreement No. 633053. The views and opinions expressed herein do not necessarily reflect those of the European Commission. The work of R. Calado has been funded by the Fundação para a Ciência e a Tecnologia (FCT, Lisboa) under Grant No. PD/BD/142967/2018 and carried out as part of his training in the framework of the Advanced Program in Plasma Science and Engineering (APPLAuSE, sponsored by FCT under Grant No. PD/00505/2012) at Instituto Superior Técnico (IST). This work has also been funded by FCT under Project No. UIDB/04561/2020. The views and opinions expressed herein do not necessarily reflect those of FCT, of IST, or of their services.

ORCID iDs

R. Calado https://orcid.org/0000-0002-7716-2230
F. Nabais https://orcid.org/0000-0003-4644-2827
S.E. Sharapov https://orcid.org/0000-0001-7006-4876
João P.S. Bizarro https://orcid.org/0000-0002-0698-6259

References

[1] Jacquinot J. *et al* 1999 ITER Physics Basis, Chapter 5: Physics of energetic ions *Nucl. Fusion* **39** 2471–95
[2] Fasoli A. *et al* 2007 Progress in the ITER Physics Basis Chapter 5: Physics of energetic ions *Nucl. Fusion* **47** S264
[3] Sharapov S.E. *et al* 2008 *Fusion Sci. Technol.* **53** 989–1022
[4] Goedbloed J.P., Holties H. A., Poedts S., Huysmans G.T.A. and Kerner W. 1993 *Plasma Phys. Control. Fusion* **35** B277
[5] Sharapov S.E., Testa D., Alper B., Borba D.N., Fasoli A., Hawkes N.C., Heeter R.F., Mantsinen M. and von Hellermann M. G. 2001 *Phys. Lett.* A **289** 127–34
[6] Fasoli A., Testa D., Sharapov S., Berk H.L., Breizman B., Gondhalekar A., Heeter R.F. and Mantsinen M. 2002 *Plasma Phys. Control. Fusion* **44** 159–72
[7] Sharapov S.E. *et al* 2002 *Phys. Plasmas* **9** 2027–36
[8] Sharapov S.E. *et al* (JET-EFDA Contributors) 2004 *Phys. Rev. Lett.* **93** 165001
[9] Fredrickson E.D. *et al* 1995 *Nucl. Fusion* **35** 1457
[10] Fu G.Y. *et al* 1998 *Phys. Plasmas* **3** 4036
[11] Saigusa M., Kimura H., Kusama Y., Kramer G.J., Ozeki T., Moriyama S., Oikawa T., Neyatani Y. and Kondoh T. 1998 *Plasma Phys. Control. Fusion* **40** 1647–59
[12] Kramer G.J., Cheng C.Z., Fu G.Y., Kusama Y., Nazikian R., Ozeki T. and Tobita K. 1999 *Phys. Rev. Lett.* **83** 2961
[13] Bernabei S. *et al* 1999 *Phys. Plasmas* **6** 1880
[14] Kramer G.J., Sharapov S.E., Nazikian R., Gorelenkov N.N. and Budny R.V. 2004 *Phys. Rev. Lett.* **92** 015001
[15] Nabais F., Borba D., Garcia-Muñoz M., Johnson T., Kiptily V. G., Reich M., Nave M.F.F., Pinches S.D. and Sharapov S.E. (JET-EFDA Contributors) 2010 *Nucl. Fusion* **50** 115006
[16] Gassner T., Schoepf K., Sharapov S.E., Kiptily V. G., Pinches S.D., Hellesen C. and Eriksson J. 2012 *Phys. Plasmas* **19** 032115
[17] Berk H.L., Borba D.N., Breizman B.N., Pinches S.D. and Sharapov S.E. 2001 *Phys. Rev. Lett.* **87** 185002
[18] Breizman B.N., Berk H.L., Pekker M.S., Pinches S.D. and Sharapov S.E. 2003 *Phys. Plasmas* **10** 3649–60
[19] Abel I.G., Breizman B.N. and Sharapov S.E. (JET-EFDA Contributors) 2009 *Phys. Plasmas* **16** 102506
[20] Nazikian R., Kramer G.J., Cheng C.Z., Gorelenkov N.N., Berk H.L. and Sharapov S.E. 2003 *Phys. Rev. Lett.* **91** 125003
[21] Sandquist P., Sharapov S.E., Lisak M. and Johnson T. 2007 *Phys. Plasmas* **14** 122506
[22] Brix M., Hawkes N.C., Boboc A., Drozdov V. and Sharapov S.E. 2008 *Rev. Sci. Instrum.* **79** 10F325
[23] Huysmans G.T.A., Goedbloed J.P. and Kerner W. 1991 *Computational Physics: Proc. CP90 Int. Conf.* (Amsterdam) September 1990 (Singapore: World Scientific) p 371
[24] Mikhailovskii A.B., Huysmans G.T.A., Kerner W.O.K. and Sharapov S.E. 1997 *Plasma Phys. Rep.* **23** 844–57
[25] Borba D. and Kerner W. 1999 *J. Comput. Phys.* **153** 101–38
[26] Fu G.Y., Cheng C.Z. and Wong K.L. 1993 *Phys. Fluids* B **5** 4040–50